International Information and Engineering Technology Association
Advancing the World of Information and Engineering

Black Widow Optimization-Based PV Array Reconfiguration for Maximized Water Flow in Agricultural Systems Under Partial Shading

Saliha Aoufi[1*], Cherif Larbes[1], Aissa Chouder[2], Abdelouadoud Loukriz[3]

[1] Laboratoire des Dispositifs de Communication et de Conversione Photovoltaïque, Ecole Nationale Polytechnique, Algiers 16200, Algeria
[2] Electronic Department, University of M'sila, M'sila 28000, Algeria
[3] Department of Electrical Engineering, University of Sciences and Technology Houari Boumediene, Algeries 16111, Algeria

Corresponding Author Email: saliha.aoufi@g.enp.edu.dz

ABSTRACT

In regions where conventional energy sources are inaccessible, unreliable, or expensive, using photovoltaic (PV) technology in agricultural water pumping systems is a viable solution for sustainable irrigation. However, the efficiency of PV systems may be significantly affected by partial shading conditions (PSCs), which can lead to degrading PV system performance, hence reducing power production. In this paper, the challenge of partial shading (PS) is addressed by proposing a new approach that combines Black Widow optimization (BWO) algorithm-based dynamic PV array reconfiguration, Kalman filter (KF)-based maximum power point tracking (MPPT), and direct torque control (DTC) for a pumping induction motor (IM). The dynamic reconfiguration algorithm exploits real-time irradiance data to optimize the output power of the PV array by adjusting module configurations, resulting in smoother power-voltage (P-V) curves and system efficiency improvement. Simulation studies are conducted and the results demonstrated the effectiveness of the proposed approach in increasing water flow and ensuring reliable operation under various PSCs. The most significant result of this research is the remarkable increase in water flow, with a gain of 432 l/h observed in one of the case studies. Considering the performance improvement the of PV water pumping system, this research may contribute to the promotion of sustainable agricultural practices, particularly in regions where access to conventional energy sources is limited.

1. INTRODUCTION

Innovation and technology play a crucial role in improving agricultural productivity. One notable area where significant progress is being made is the integration of sensors into agriculture, a trend of the utmost importance. Agriculture is an essential sector of the economy in many countries. At present, a considerable number of farmers rely on traditional sources such as mains electricity or diesel engines for their water pumping needs [1]. However, the expense of diesel pumping has become increasingly onerous. In addition, large tracts of farmland are located in remote areas without electricity [2, 3]. Even in areas with access to electricity, demand for water increases during the summer months, often coinciding with power cuts. Thus, the adoption of PV water pumping appears to be a practical solution to conserve energy, relieve pressure on the electricity grid, and reduce energy costs in the long term.

Partial shading conditions (PSCs) are a major challenge to the efficiency of solar water pumping systems [4, 5]. These conditions are typically caused by obstacles such as trees, tall grass, bushes, telephone poles, birds, hills, and rocks that cast shadows on nearby PV modules [6]. Permanent shading of PV modules in the same area can lead to hot spots and potential damage. To mitigate this, bypass diodes are usually installed on PV modules to avoid this situation. However, this configuration often leads to multiple peaks in the output, significantly reducing the overall power output of the PV array [7]. Various PV array topologies, such as total-cross-tied (TCT) and honeycomb (HC), have been developed to minimize mismatch losses and improve efficiency. Of these topologies, TCT has been shown to generate the highest power output under most shading conditions [7, 8]. However, no single topology consistently outperforms the others in all shading scenarios. Therefore, several static and dynamic reconfiguration methods have been proposed in the literature to improve the PV arrays' output power [9].

Static reconfiguration algorithms use puzzle patterns to disperse shading effects [10]. These algorithms have proven effective for recurring shading scenarios. However, with advances in sensors, solid-state devices, and high-end processors, dynamic reconfiguration is emerging as an enviable solution to counter the impact of partial shading conditions [10-12]. Researchers mainly apply dynamic reconfiguration to TCT configurations, focusing on irradiance equalization to improve output power [13, 14]. This improvement in output power directly increases the efficiency

of photovoltaic pumping systems. PV array dynamic reconfiguration technology, which is particularly well suited to water pumping applications due to its ability to scale to smaller PV arrays, cane improve power output under various shading conditions [15]. In addition, the P-V characteristics obtained by dynamic reconfiguration are more consistent, allowing the PV water pumping system to use conventional MPPT techniques for optimal energy extraction.

The P-V curve of a PV module has ae distinct point where maximum power is delivered. MPPT techniques precisely track this point to optimize the PV module's efficiency. There are a variety of MPPT algorithms for extracting maximum power from PV panels [16]. Conventional methods include perturbation and observation (P&O) and incremental conductance (I&C). Hybrid and optimization-based MPPT algorithms offer even more accurate tracking capabilities. Numerous researchers have explored various soft computing and intelligent approaches for MPPT. Notable methods include the Kalman filter (KF) [17], fuzzy logic control (FLC) [18], artificial neural networks (ANN) [19], particle swarm optimisation (PSO) [20], ant colony optimisation (ACO) [21], and the artificial bee colony (ABC) algorithm [22]. These techniques are known for their rapid response when applied to MPPT tasks. Among them, the KF-based MPPT stands out due to its effective use of recursive filtering, leveraging estimations of previous, current, and potentially future states while handling noisy data measurements. In contrast, the Black Widow Optimization (BWO) algorithm—an emerging evolutionary algorithm inspired by the unique mating behavior of black widow spiders—demonstrates superior exploration–exploitation balance, faster convergence, and lower computational complexity [23, 24]. These characteristics make it particularly well-suited for real-time PV array reconfiguration under rapidly varying partial shading scenarios. To the best of our knowledge, this is the first study to apply BWO for dynamic PV array reconfiguration in a TCT topology, offering an original contribution to the field of intelligent PV system control.

Extensive research has been conducted on photovoltaic (PV) water pumping systems, focusing primarily on two main configurations: single-stage and two-stage setups [25-28]. Managing the DC link in single-stage configurations poses significant challenges [28]. Nevertheless, single-stage designs are often preferred for their higher efficiency, stemming from the use of fewer components [26]. Conversely, two-stage power conversion systems provide enhanced flexibility in terms of design, operation, and control. Early studies on solar water pumping predominantly utilized DC motors, which were chosen for their straightforward compatibility with PV arrays [29]. However, these motors typically require frequent maintenance. To address this issue, researchers are investigating the use of advanced magnetic materials in the development of motors tailored to specific applications [30]. These modern motors demonstrate high efficiency and have lower maintenance needs [31], though the substantial cost of magnetic materials contributes to the overall expense of the motor. Other open-wound induction motors (IMs) have also been used for this purpose [27, 31], but their practical availability is problematic. Despite this, IMs remain popular due to their reliability, high availability, robust construction, affordability, and direct compatibility with pump loads [28, 32]. However, the integration of dynamic PV array reconfiguration based on black widow optimization, Kalman filter (KF)-based MPPT controller, and direct torque control

(DTC) using a two-level inverter to regulate IMs under PSCs has not previously been explored.

This paper introduces an innovative method for dynamically reconfiguring PV arrays using sensors and switches, aimed at optimizing the output power of TCT PV arrays under partial shading conditions (PSCs). Additionally, a Kalman filter algorithm is employed for MPPT, and direct torque control (DTC) with space vector pulse width modulation (SVPWM) is applied to drive the induction motor (IM) pump. The primary goal of this study is to enhance the performance of PV water pumping systems under PSCs.

The key contributions of this research are outlined as follows:

1. A novel dynamic reconfiguration strategy based on the BWO algorithm is proposed. This algorithm is chosen over other metaheuristics for its superior convergence speed and robustness in handling complex shading conditions. It uses real-time irradiance data to adjust the configuration of PV modules in a TCT array via switches, ensuring maximum power delivery under all PSC scenarios.

2. An MPPT controller based on the KF is adopted to mitigate the occurrence of multiple peaks on the P-V curve, resulting in smoother P-V curves. Typically, under PSCs, conventional MPPT algorithms such as Perturb and Observe (PO) and Incremental Conductance (IC) fail to efficiently track the global MPP. However, with the proposed algorithm, this problem is solved, allowing the MPPT algorithm to perform optimally even under PSCs, thus ensuring efficient system operation.

3. A control scheme including the proposed PV reconfiguration method and KF-based MPPT controller is applied for an IM pumping system with a DTC controller. The results show that an increase of the PV array power under PSCs is achieved which contributes to an enhancement of the water discharge with a gain of 423 l/h.

The rest of this paper is organized as follows: Section 2 presents the design and analysis of the system under study in greater detail. Section 3 describes the adopted control scheme, including the proposed photovoltaic (PV) reconfiguration method and some relevant aspects. Section 4 analyzes the simulation results. Finally, Section 5 summarizes the main conclusions.

2. DESIGN AND MODELING OF THE ADOPTED SYSTEM

The schematic diagram of the adopted system is shown in Figure 1, including a partially shaded TCT PV array, a switching matrix, power electronic converters (DC-DC boost and DC-AC two-level inverter), and an IM pump with their control part. A detailed system analysis is provided in this section, describing the principle of operation of the solar PV water pumping system (SPVWPS).

The setup begins with the motor design, followed by the arrangement of the TCT PV array, the switch network, and the integration of converters.

2.1 Model of IM

The IM mathematical model in the stationary reference ($\alpha\beta$) frame is given by the following equations [33]:
- The stator voltages:

$$\begin{cases} V_{s\alpha} = R_s I_{s\alpha} + \dfrac{d\emptyset_{s\alpha}}{dt} \\ V_{s\beta} = R_s I_{s\beta} + \dfrac{d\emptyset_{s\beta}}{dt} \end{cases} \quad (1)$$

- The stator flux:

$$\begin{cases} \emptyset_{s\alpha} = L_s I_{s\alpha} + M I_{r\alpha} \\ \emptyset_{s\beta} = L_s I_{s\beta} + M I_{r\beta} \end{cases} \quad (2)$$

- The rotor voltages:

$$\begin{cases} 0 = R_r I_{s\alpha} + \dfrac{d\emptyset_{r\alpha}}{dt} + \emptyset_{r\beta} \\ 0 = R_r I_{s\beta} + \dfrac{d\emptyset_{r\beta}}{dt} + \emptyset_{r\alpha} \end{cases} \quad (3)$$

- The rotor flux:

$$\begin{cases} \emptyset_{r\alpha} = L_s I_{r\alpha} + M I_{s\alpha} \\ \emptyset_{r\beta} = L_s I_{r\beta} + M I_{s\beta} \end{cases} \quad (4)$$
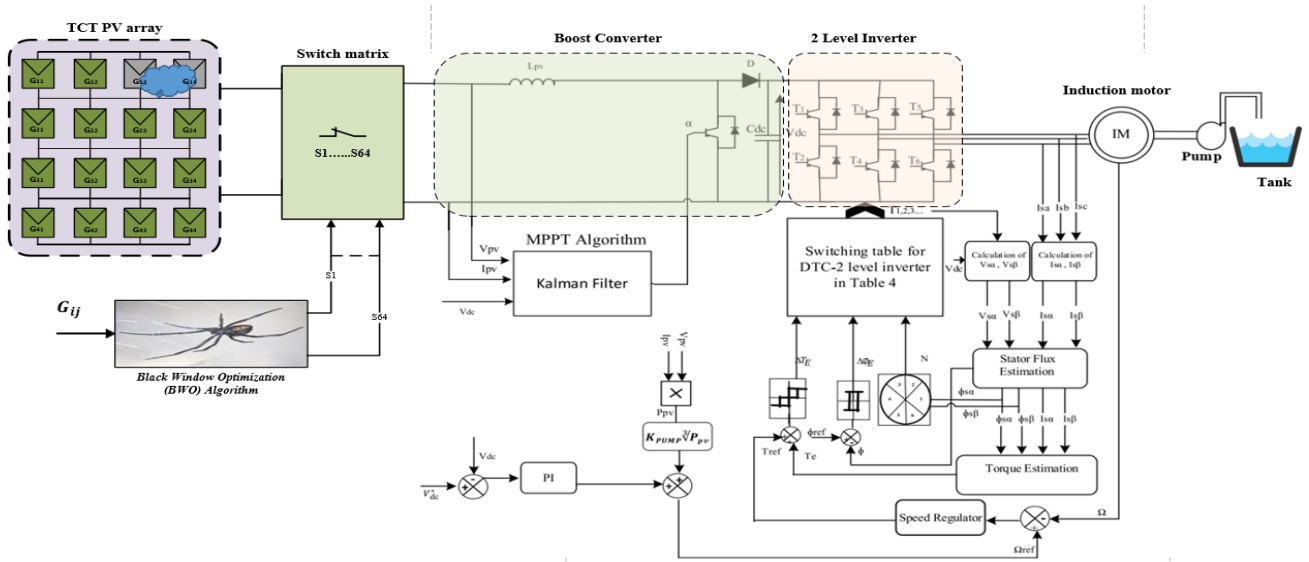

Figure 1. Block diagram illustrating the proposed water pumping system utilizing a reconfiguration-based BWO algorithm

In this context, $I_{s\alpha}$, $I_{s\beta}$, $I_{r\alpha}$, and $I_{r\beta}$ denote the stator and rotor currents in the $\alpha\beta$ reference frame, respectively. M represents the mutual inductance, while L_s and L_r correspond to the stator and rotor inductances. Additionally, R_s and R_r signify the stator and rotor resistances.

The electromagnetic torque expression in the $\alpha\beta$ reference frame is given by:

$$T_e = \frac{3}{2} \times p\big(I_{s\beta}\emptyset_{s\alpha} - I_{s\alpha}\emptyset_{s\beta}\big) \quad (5)$$

The specifications of the IM used are shown in Table 1.

Table 1. Induction motor parameters

Parameters	Values
Rated Power (P) [kW]	1.5
Rated Speede (Ω) [rpm]	1420
Nominal Frequency (f) [Hz]	50
Stator Resistance (Rs) [Ω]	4.850
Rotor Resistance (Rr) [Ω]	3.805
Stator Inductance (Ls) [H]	0.274
Rotor Inductance (Lr) [H]	0.274
Mutual Inductance (M) [H]	0.258
Number of Pole Pairs (P)	2
Rated Voltage [V]	230

2.2 PV array

To ensure the proper functioning of the PV solar water pumping system, it is essential that the power capacity of the PV array exceeds that of the induction motor (IM). Consequently, a 2.4kW TCT (4×4) photovoltaic array is selected to power the chosen IM. The current for the TCT array is determined using the method outlined in reference [34]:

$$I_{ij(shaded)} = K I_{ij(STC)} \quad (6)$$

where,

$$K = \frac{G_{ij}}{G_{STC}} \quad (7)$$

In this context, i and j represent the row and column indices of the array. I_{ij} (shaded) and I_{ij} (standard) denote the current of the PV module under shaded and standard irradiance conditions ($1000 W/m^2$), respectively. G_{ij} represents the irradiance incident on the ij-th module, while G_{STC} refers to the standard test condition irradiance. The voltage of the PV array is given by [6]:

$$V_{PV} = \sum_{i=1}^{m} V_i \quad (8)$$

where, m denotes the total number of rows, ie represents the specific row number, v_i is the voltage of the i-th row, and V_{pv} represents the overall voltage of the array. The detailed specifications of the PV module and the PV array are provided in Table 2.

Table 2. PV system characteristics

	PV Module	PV Array
Maximum power (P_{mpp}) [W]	150	2400
Maximum current (I_{mpp}) [A]	4.35	17.4
Maximum voltage (V_{mppv}) [V]	34.6	138.4
Open circuit voltage (V_{oc}) [V]	43.6	174.4
Short circuit current (I_{sc}) [A]	4.85	19.4

2.3 Calculation of irradiance using sensors and single-pole single-throw switches

The electrical diagram of the switching matrix of the proposed method for optimizing the power of the PV array initially configured as a TCT structure is shown in Figure 2. The positions of the solar PV modules in the TCT structure can be changed using a reduced number of switches. As a result, each PV module requires one bipolar switch for each line. Here, the number of switches required is given by the following equation [34]:
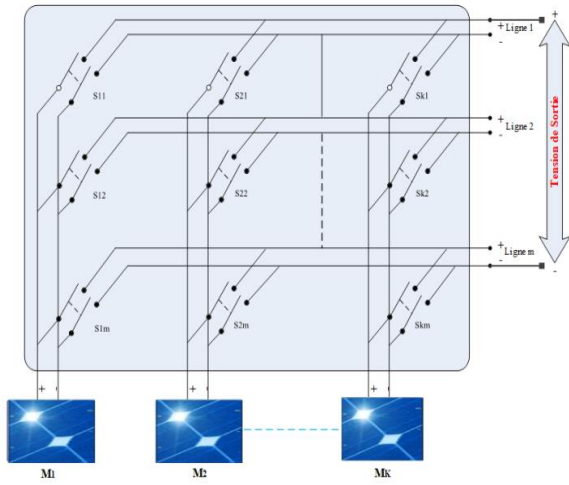

Figure 2. Electrical circuit diagram of the used switching matrix [34]

$$S_{TCT} = n \times m^2 \tag{9}$$

where, S$_{TCT}$ denotes the total number of bipolar switches required, and m and n represent the number of rows and columns in the TCT PV array, respectively. Consequently, the required number of pyrometer sensors is given by:

$$P_G = N \tag{10}$$

where, PG represents the number of irradiation sensors (pyrometers) and N denotes the total number of PV modules.

2.4 Design and analysis of the DC-DC boost converter for system optimization

The design of the DC-DC boost converter is a critical factor in optimizing the performance of the system. In particular, the values of the duty cycle α, the inductor L_{pv}, and the capacitor C_{dc} need to be determined using the continuous conduction mode (CCM) [35]. The duty cycle α, governs the operation of the converter and plays a significant role in regulating the output voltage. To calculate α, the following expression is used:

$$\alpha = \frac{V_{dc} - V_{mppv}}{V_{dc}} \tag{11}$$

The boost converter inductance is calculated as follows:

$$L_{pv} = \frac{V_{mppv}\alpha}{\Delta I f_s} \tag{12}$$

where, f_s is the switching frequency and ΔI is the current maximum ripples.

The DC bus voltage at the inverter input voltage, V_{dc}, can be calculated as follows:

$$V_{dc} = \frac{2\sqrt{3}V_{LL}}{\sqrt{3}} \tag{13}$$

where, V_{LL} represents the RMS (Root Mean Square) line voltage of the IM.

The value of the capacitor for the DC bus is calculated using the following equation, which takes into account the system's voltage fluctuations and energy storage requirements:

$$C_{dc} = \frac{6 \, \alpha V_{LL} I_L t}{\sqrt{3} \, (V_{dc}^{*2} - V_{dc}^2)} \tag{14}$$

where, V_{dc}^* and V_{dc} denote the reference and measured values of the DC bus voltage, respectively, t represents the time duration over which the DC link voltage is adjusted, α is the duty cycle that controls the converter's operation, and I_L refers to the line current of the IM, which plays a crucial role in determining the power delivered to the motor.

The calculated parameters of the boost converter are listed in Table 3.

Table 3. DTC switching table powered by a two-level inverter

Torque ΔTe / Sector (Ts)	Flux Δϕs = 1			Flux Δϕs = 0		
	ΔTe = 1	ΔTe = 0	ΔTe = −1	ΔTe = 1	ΔTe = 0	ΔTe = −1
1	V2	V0	V6	V3	V0	V5
2	V3	V0	V1	V4	V0	V6
3	V4	V0	V2	V5	V0	V1
4	V5	V0	V3	V6	V0	V2
5	V6	V0	V4	V1	V0	V3
6	V1	V0	V5	V2	V0	V4

2.5 Centrifugal pump

The load torque of a centrifugal pump (T_{pump}) is proportional to the square of the IM speed (Ω), as shown in Eq. (15) [36]:

$$T_{pump} = K_{pump} \, \Omega^2 \tag{15}$$

with K_{pump} representing the centrifugal pump constant.

3. PROPOSED CONTROL SCHEME

In this section, the proposed control for the PV pumping system is described in detail. First, the proposed BWO algorithm for dynamic reconfiguration with the KL-based

MPPT technique is presented. Next, the IM modeling and its control scheme are provided.

3.1 Black widow optimization (BWO)-based PV array reconfiguration

In conventional PV systems, series-parallel or TCT configurations are commonly employed to meet specific load demands [37]. Among these, the TCT configuration has proven particularly effective under PSCs due to its superior performance in mitigating mismatch losses. In this work, a dynamic reconfiguration strategy is proposed to further enhance the performance of TCT-connected PV arrays using the Black Widow Optimization (BWO) algorithm. The reconfiguration mechanism relies on real-time irradiance data from each module, collected through sensors. These measurements are used to generate switching control signals that adjust the interconnections between modules. The objective is to dynamically rearrange the modules to optimize the irradiance distribution and extract the maximum possible power from the array under shading.

3.1.1 Overview of the BWO algorithm

The BWO algorithm is a population-based metaheuristic optimization technique that operates using mechanisms analogous to selection, reproduction, and mutation [23, 24]. It does not depend on biological fidelity but instead utilizes abstracted computational procedures to explore the solution space efficiently. Each solution, or individual, represents a candidate configuration for the PV array.

3.1.2 Initial population

The population is initialized with randomly generated candidate solutions:

$$W = \left[X^1, X^2, \dots, X^{N^{Var}} \right] \qquad (16)$$

where, $X^{N^{Var}}$ represents the number of decision variables (i.e., PV module positions), and each X^i, denotes a floating-point vector encoding a possible interconnection layout of the modules.

3.1.3 Fitness function evaluation

The objective of the optimization process is to minimize power mismatch between array rows, thereby maximizing total power output. This is mathematically formulated through a fitness function that minimizes the difference in total irradiance received by each row:

$$fitness = \text{minimize}\big(max(sumG(n,1)) \\ - min(sumG(n,1)) \big) \qquad (17)$$

This formulation ensures that rows receive similar irradiance levels, thereby equalizing current outputs and minimizing bypass diode activation.

3.1.4 Reproduction and cannibalism mechanism

High-quality individuals (configurations with better fitness) are selected for mating through a crossover operator. New offspring are generated by combining portions of parent solutions. To maintain population diversity and improve convergence, a selection pressure mechanism is applied: a portion of the lowest-performing individuals is removed from

the population (analogous to the biological concept of cannibalism, though abstracted here as an elimination step).

3.1.5 Mutation and replacement

To avoid premature convergence and local minima, a low-probability mutation operation is applied to certain solutions, introducing new variability into the population. The best-performing individuals are retained for the next generation.

3.1.6 Implementation in PV array reconfiguration

In this study, the BWO algorithm interfaces with a switching matrix responsible for modifying the physical connections between PV modules. At each reconfiguration interval, the algorithm processes the irradiance data and returns the optimal layout that maximizes the array's power output under the current PSC scenario.

The complete process of the proposed BWO-based PV array reconfiguration is illustrated in Figure 3.
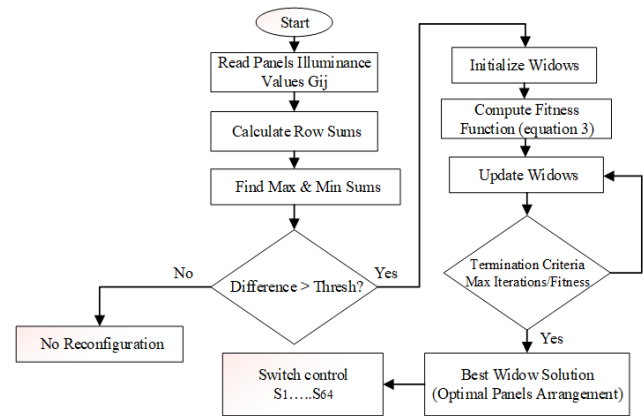

Figure 3. Flowchart of the BWO Algorithm for dynamic PV array reconfiguration

3.2 Kalman filter-based MPPT control algorithm

Enhancing the energy efficiency of the SPVWPS relies heavily on the performance of the MPPT controller, which is essential for optimizing the power output of PV cells across varying environmental conditions. The voltage-power and voltage-current characteristics of the solar panel change with different levels of irradiance, revealing that each shift in irradiance results in a new maximum power point (V_{mpp}, I_{mpp}). To effectively track these changes, the KF is utilized in the MPPT process, with its specific operating principles detailed in the following sections. An iterative KF approach is applied to estimate state variables by refining predictions derived from noisy measurement data. This process involves two key phases that are repeated at each iteration: the prediction phase (temporal updates) and the correction phase (measurement updates). These iterative adjustments continue until an accurate representation of the measured value is achieved. During the prediction phase, the KF projects the future state and estimates the error covariance, resulting in a priori predictions for the next iteration. The underlying mathematical expressions for this prediction process are as follows [38]:

- Forecast the state for the upcoming step

$$x_k^- = A x_{k-1} + B u_{k-1} \qquad (18)$$

- Project the covariance error

$$P_k^- = AP_{k-1}A^T + Q \qquad (19)$$

In the Kalman filter (KF) algorithm, x_k^- represents the predicted state estimate at iteration k, derived from the state estimate x_{k-1} from the previous iteration using the measurement z_{k-1}. The term A denotes the transitione state constante modele appliede toe thee prior estate, while Be ise ae constante corresponding to the econtrol-input emodel used for the control process. The control input at iteration k-1 is denoted by u_{k-1}. The variable P_k^- indicates the prior error covariance at iteration k, P_{k-1} is the posterior error covariance from iteration k-1, and Q represents the process noise covariance linking the prior and posterior error covariances.

The correction phase of the KF algorithm involves three main equations for refining the predicted value [17]:

• Kalman Gain Calculation:

$$K_k = H_k^- C^T (CH_k^- C^T + R)^{-1} \qquad (20)$$

• Estimate Update Using Measurement:

$$x_k = x_k^- + K_k(z_k - Cx_k^-) \qquad (21)$$

• Covariance Error Update:

$$P_k = (I - P_k C)P_k^- \qquad (22)$$
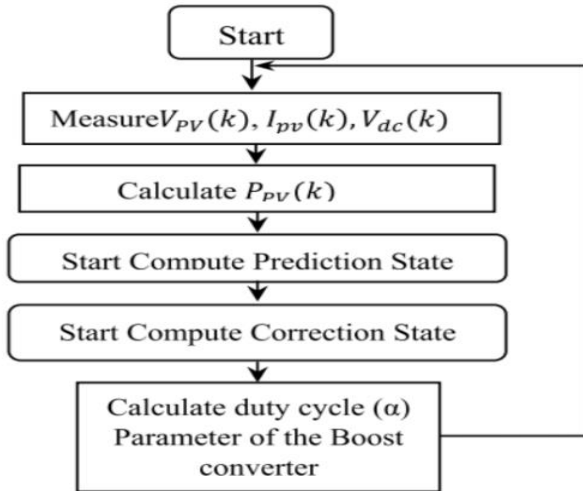
Figure 4. Flowchart of the MPPT algorithm utilizing a kalman filter

In these equations, x_k is the corrected state at iteration k based on the measurement z_k, R is the measurement noise covarianc, Kk is the Kalman gain, Ce is a system constant dependent on the KF frame work and the observed data space, and Pk erepresents the posterior error covariance ate iteration k. For Maximum Power Point Tracking (MPPT), the KF algorithm must monitor the operating point's position in real time, adjusting to environmental changes such as variations in irradiance and temperature impacting thee PVe arrays. According to the P-Ve curve, power increases withe a positive slope until reaching the MPP, followed by a decrease with a negative slope beyond that point. The KF uses its predictive and corrective equations toe derive the optimal duty cycle (α) for the DC-DC boost converter, ensuring the PV system operates at the MPP. Thee flowchart of the KF-based MPPT algorith is shown in Figure 4.

3.3 DTC control for IM using a two-level inverter

The DTC strategy controls the two-level inverter switches toe drivee the IM. By selecting one of eight voltage vectors (six active: V1-V6, and two zero: V0, V7), the inverter's state is determined. These vectors are divided into six 60-degree sectors, as depicted in Figure 5. The optimal voltage vector is chosen based on the motor's flux position and the desired changes in flux and torque magnitude, as outlined in Table 3 [39]. Figure 6. Flowchart illustrating the implementation of the direct torque control (DTC) strategy in a two-level inverter-fed induction motor. The flowchart includes flux and torque estimation, hysteresis control, sector identification, and voltage vector selection.
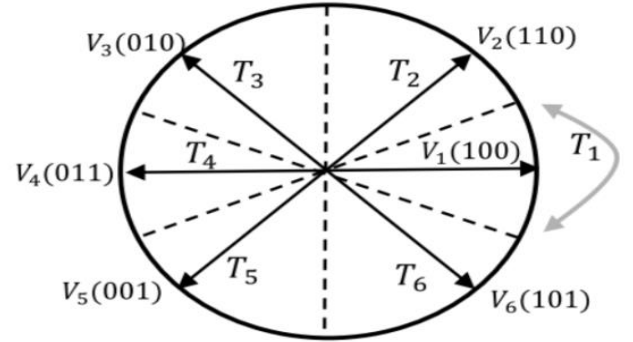

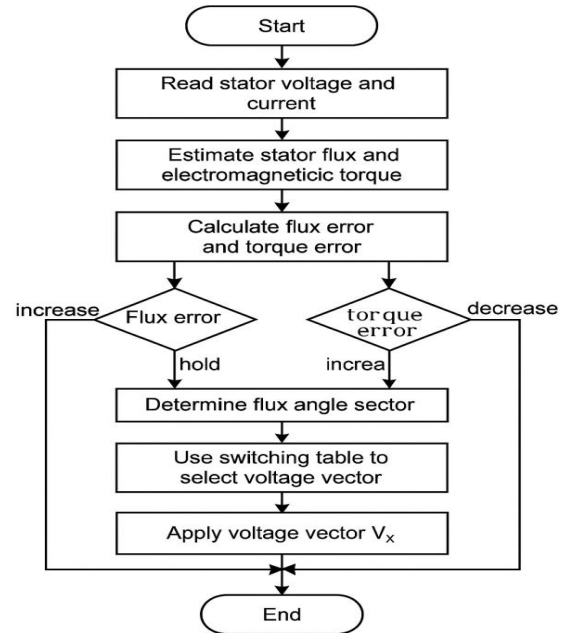**Figure 5.** Space voltages for two-level inverter

Figure 6. DTC strategy for a two-level inverter driving an induction motor

4. SIMULATION RESULTS

The proposed system is modeled and simulated in Matlab/Simulink for three PSC cases.
Case 1: Considering the shading issue illustrated in Figure 7 (a), the surface of the PV array of 16 PV modules interconnected in TCT experiences varying irradiance levels,

including 1000W/m², and 600W/m². Within this scenario, significant shading occurs, encompassing the array's modules, particularly affecting the first row.
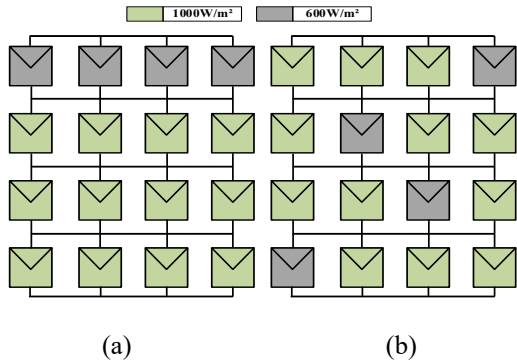

(a)   (b)

Figure 7. Shade dispersion for case 1, (a) TCT configuration, and (b) proposed BWO-based PV arrangement
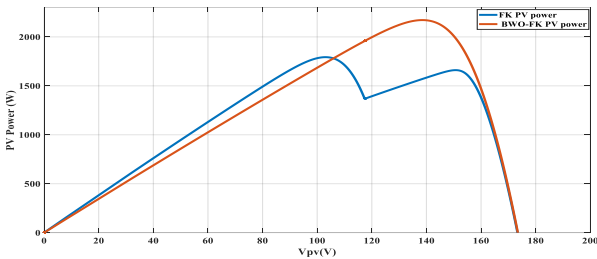

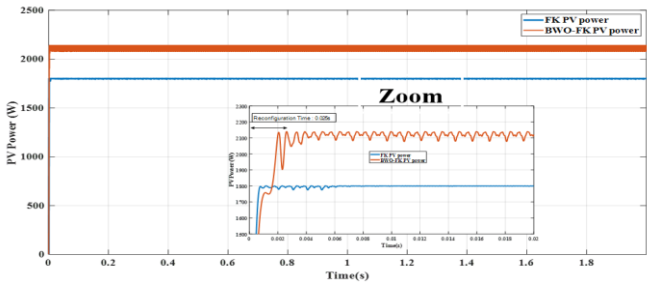**Figure 8.** PV characteristics acquired through the TCT and the proposed BWO algorithm for case 1

Figure 9. PV array power before (FK PV power) and after reconfiguration (BWO-FK PV power) for case 1

To calculate the output power, the switch matrix configuration shown in Figure 7 (b) is utilized. By altering the module positions, this matrix optimizes PV output power. The reconfigured array is depicted in Figure 7 (b), and its P-V characteristics are graphically illustrated in Figure 8. The results validate the efficacy of the BWO-based reconfiguration strategy. This approach effectively distributes shadow levels across the PV array, leading to consistent PV characteristics and minimized row current disparities. Notably, the BWO algorithm generates a power output of 2170 W, surpassing the initial TCT interconnection's 1793 W. Additionally, the BWO configuration exhibits a single Maximum Power Point (MPP), unlike the initial TCT arrangement's two MPPs. This reduced number of MPPs positively impacts the MPPT algorithm's accuracy. Figure 9 presents the PV array power response before and after BWO-based reconfiguration. A significant power increase of over 24% is observed post-reconfiguration.

The delay in this response is attributed to the PV array's reconfiguration time.

Figure 10 illustrates the electromagnetic torque (Te) response of the PV array with and without BWO-FK reconfiguration. Simulation results indicate that reconfiguration reduces torque ripple, leading to smoother operation. Figure 11 depicts the rotor speed evolution using BWO reconfiguration. This figure demonstrates that the rotor speed under PSCs is significantly improved with BWO reconfiguration (over 162 rad/s), compared to the initial configuration with simple FK-based MPPT without reconfiguration (around 143 rad/s). Figure 12 shows the water flow time evolution. The results indicate that the quantity of pumped water under PSCs using the proposed reconfiguration method is increased by more than 14%.
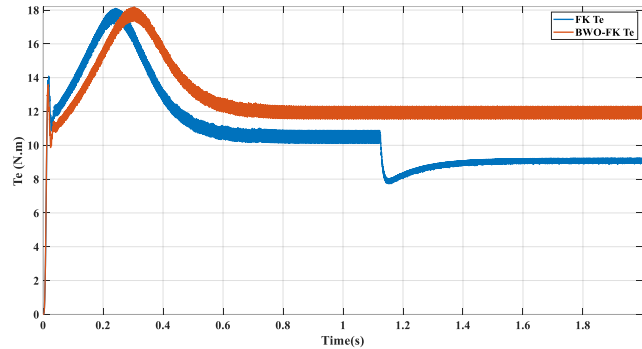

Figure 10. Electromagnetic torque response of the motor under BWO-based PV array reconfiguration for case 1
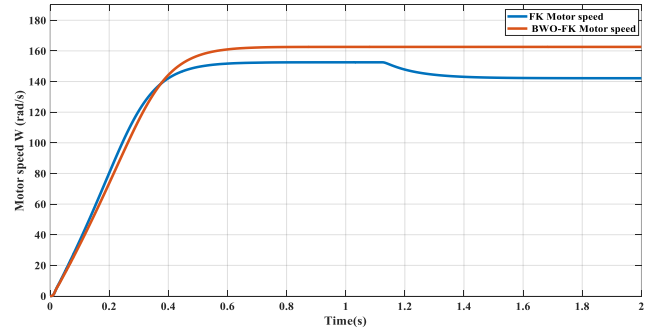

Figure 11. Motor speed before and after PV array reconfiguration using BWO algorithm for case 1
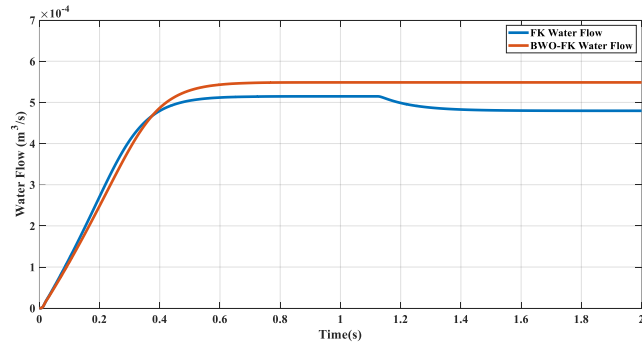

Figure 12. Water flow before and after PV array reconfiguration using BWO algorithm for case 1

Case 2: Figure 13 (a) depicts a TCT-interconnected PV array under partial shading conditions (PSCs), where three

distinct irradiation levels (200W/m², 600W/m², and 1000W/m²) are present. The arrangement shown in Figure 13 (b) leverages the BWO algorithm to improve power output. The switch matrix repositions the PV modules based on irradiance readings and switching signals from the BWO algorithm. This reconfiguration optimizes power output. Figure 14 graphically illustrates the P-V characteristics. The BWO-based reconfiguration effectively distributes shadow levels, resulting in consistent PV characteristics and minimized row current disparities. The BWO algorithm generates higher power output compared to the initial TCT interconnection, with a single Maximum Power Point (MPP) instead of two. This reduced number of MPPs positively impacts the MPPT algorithm's accuracy.
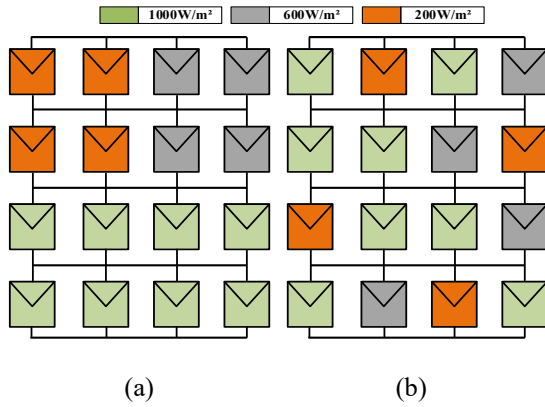

Figure 13. Shade dispersion for case 2, (a) TCT configuration, and (b) proposed BWO arrangement
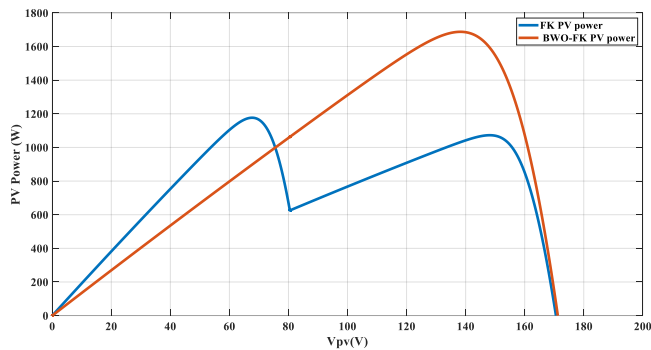

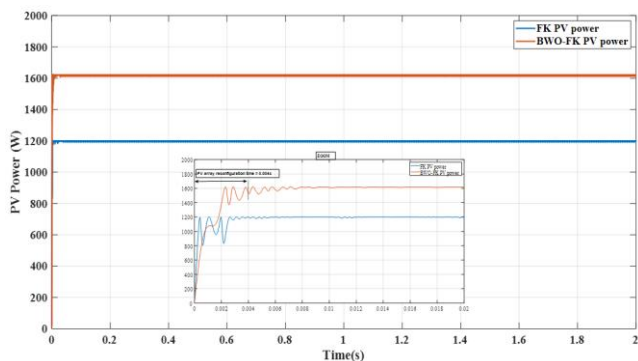**Figure 14.** PV characteristics acquired through the TCT and the proposed BWO algorithm for case 2

Figure 15. PV array power before (FK PV power) and after reconfiguration (BWO-FK PV power) for case 2
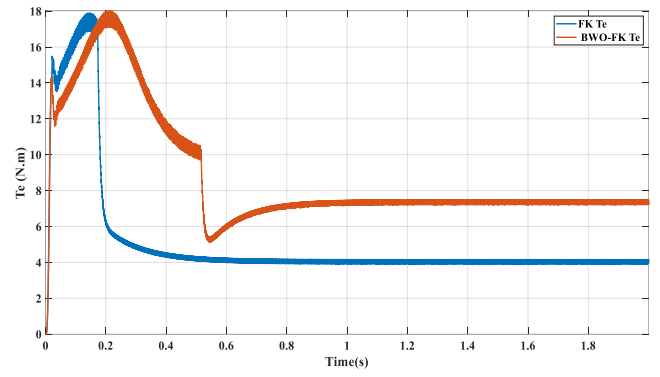

Figure 16. Electromagnetic torque response of the motor under BWO-based PV array reconfiguration for case 2
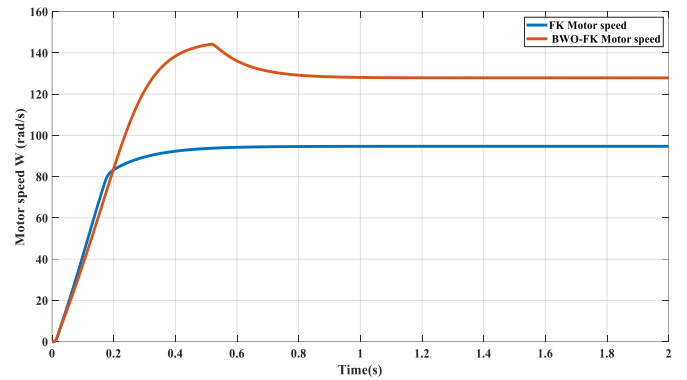

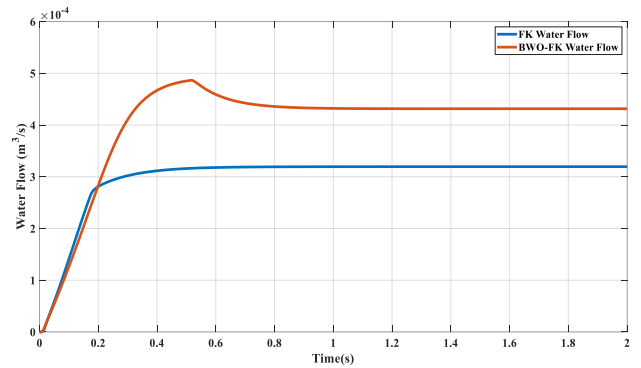**Figure 17.** Motor speed before and after PV array reconfiguration using BWO algorithm for case 2

Figure 18. Water flow before and after PV array reconfiguration using BWO algorithm for case 2

The response of the PV array power before and after reconfiguration is shown in Figure 15, where the BWO algorithm-based reconfiguration is applied. It can be seen that the PV array power increases by more than 35% after the reconfiguration. It is worth noting that the small delay is due to the reconfiguration time of the PV array.

Figure 16 compares the performance of the PV array in terms of electromagnetic torque (T_e), first without reconfiguration and with reconfiguration (BWO-FK). The simulation results highlight the benefits of reconfiguration, in reducing torque ripple and improving torque stability. Figure 17 illustrates the impact of the BWO-based reconfiguration method on the rotor speed. The simulation shows a clear improvement in the rotor speed after reconfiguration of the PV array, particularly under PSCs, exceeding 127 rad/s, in

contrast to the initial configuration, which peaked at 94 rad/s. As for the evolution of the water flow rate, presented in Figure 18, it reveals an increase of more than 38% in the quantity of water pumped under PSCs when using the proposed method. This significant increase in water flow rate demonstrates the considerable effectiveness of the proposed technique.

Case 3: Figure 19 illustrates a TCT-interconnected PV array exposed to four distinct irradiation levels (100W/m², 200W/m², 600W/m², and 1000W/m²) under PSCs. The proposed method transmits switching commands to the switch matrix, enabling module repositioning to optimize power output. Figure 20 presents the P-V characteristics, highlighting the significant effectiveness of the BWO-based reconfiguration method. This method achieves a more even distribution of shadow levels, leading to consistent PV characteristics and reduced row current disparities. The BWO algorithm generates higher power output compared to the initial TCT interconnection, with a single Maximum Power Point (MPP) instead of four. This reduced number of MPPs positively impacts the MPPT algorithm's accuracy.

The power response of the PV array before and after the application of the BWO reconfiguration is shown in Figure 21. We observe a significant increase in the power of the PV array, exceeding 44% after the implementation of the BWO reconfiguration. It is important to note that the slight delay is due to the time required to reconfigure the PV array.
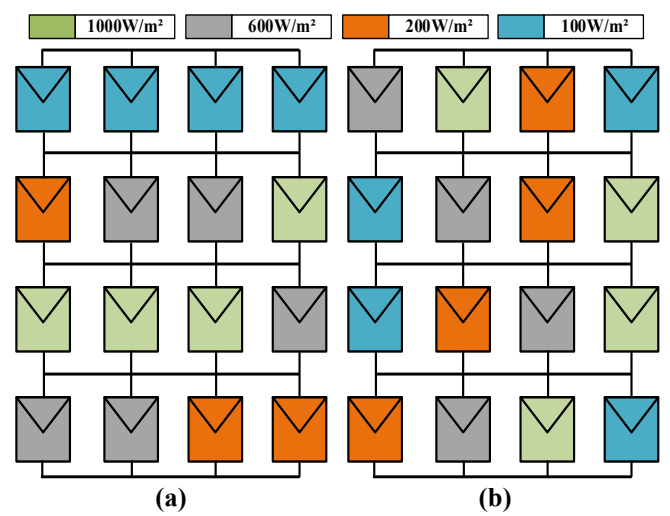
without reconfiguration and then with reconfiguration (BWO-FK). The simulation results highlight the benefits of reconfiguration in reducing torque ripple and improving torque stability. Regarding Figure 23, it highlights the impact of the proposed reconfiguration on rotor speed. The simulation shows a clear improvement in rotor speed after reconfiguration of the PV array, particularly under PSCs, where it exceeds 84 rad/s. However, the rotor speed peaked at 59 rad/s in the initial configuration with FK-based MPPT. The water flow evolution, presented in Figure 24, shows an increase of more than 40% in the amount of the water pumped under PSCs by using the proposed algorithm. Given this significant increase in water flow rate, it is clear that the proposed technique is highly effective.
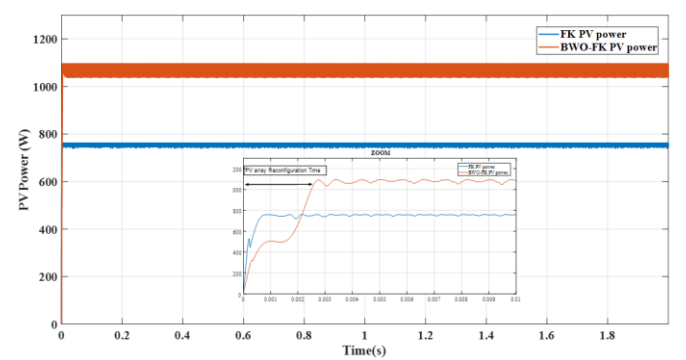
Figure 21. PV array power before (FK PV power) and after reconfiguration (BWO-FK PV power) for case 3
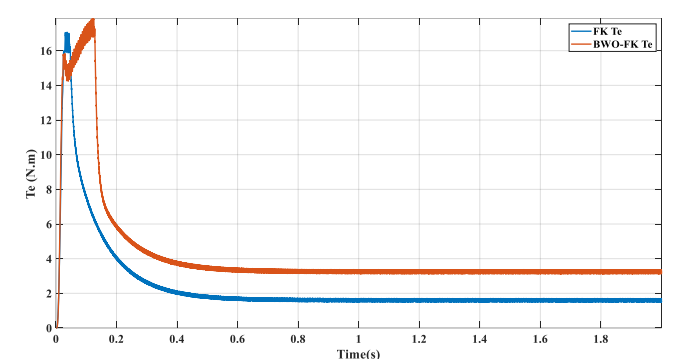
Figure 22. Electromagnetic torque of the motor before and after PV array reconfiguration using BWO algorithm for case 3

Figure 19. Shade dispersion patterns for case 3: (a) TCT interconnection, (b) BWO reconfiguration
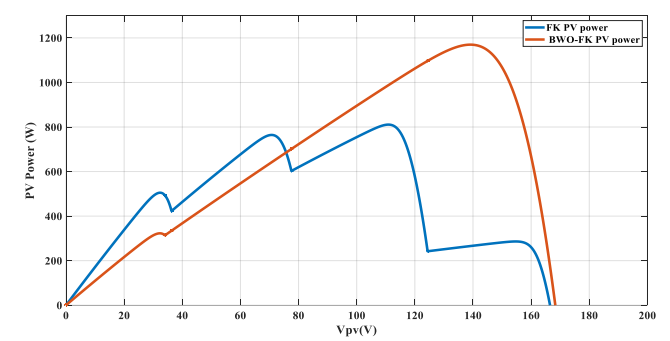

Figure 20. Power-Voltage curves of the PV array under TCT and BWO reconfiguration (case 3)

Figure 22 shows the comparison of the PV array performance in terms of electromagnetic torque, initially

Figure 23. Motor speed before and after PV array reconfiguration using BWO algorithm for case 3

Figure 24. Water flow before and after PV array reconfiguration using BWO algorithm for case 3

A comparative analysis of the overall performance indices of the SPVWPS under PSCs is presented in Table 4. The water gained formula for each case is provided in Eq. (23). The

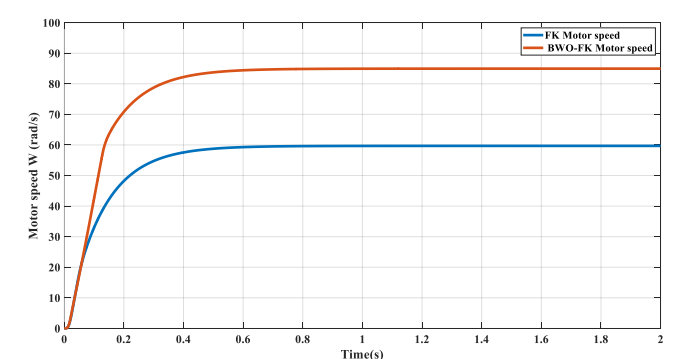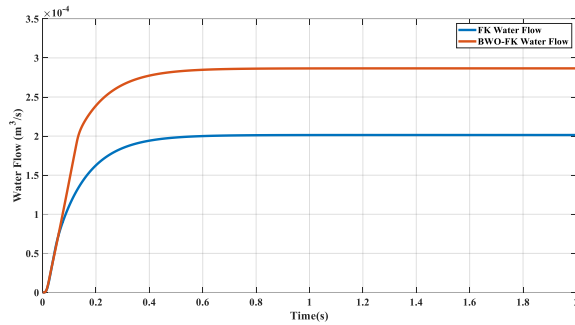superior efficiency of the proposed algorithm is evident from the performance indices in Table 4. The system demonstrates robust steady-state performance, guaranteeing reliable water evacuation even under PSCs. Moreover, the motor pump effectively tracks the Maximum Power Point (MPP) of the PV array, ensuring optimal water supply based on available solar power.

$$\text{Gained water (l/h)} = \frac{(Q_{BWO-FK} - Q_{FK}) \times 1000}{3600} \quad (23)$$

The results reveal a substantial improvement in water flow, with the following average increase: the first case observed a gain of 216 l/h, the second a gain of 432 l/h, and the third a gain of 288 l/h. By improving the performance of the PV water pumping system, this research may contribute to the promotion of sustainable agricultural practices, particularly in regions where access to conventional energy sources is limited.

Table 4. Performance comparison of SPVWPS under PSCs

No.	Cases	Used Technique	P_{pv} (W)	Ω (rad/s)	Te (N.m)	Q (m³/s)	Gained Water (l/h)
1	Case 1	Without reconfiguration	1799.9	143.01	9.12	4.8 10^{-4}	216
2		With reconfiguration (BWO-FK)	2138.46	162.59	12.26	5.4$10^{-4}$	
3	Case 2	Without reconfiguration	1197.96	94.69	4.1	3.1 10^{-4}	432
4		With reconfiguration (BWO-FK)	1621.03	128.104	7.39	4.3$10^{-4}$	
5	Case 3	Without reconfiguration	756.67	59.68	1.6	2.0 10^{-4}	288
6		With reconfiguration (BWO-FK)	1095.05	84.94	3.15	2.8$10^{-4}$	

5. CONCLUSION

This paper presented a new approach to improve the performance of a solar PV water pumping system under PSCs. By combining dynamic PV array reconfiguration using the BWO algorithm, KF-based MPPT controller, and DTC for an IM using a two-level inverter, significant progress has been made in optimizing system efficiency and reliability. The proposed BWO algorithm effectively increases the PV output power by dynamically reconfiguring the PV array in response to changing irradiation conditions, resulting in a more consistent and efficient power generation. This increase in the PV output power directly influences motor speed through the DTC mechanism, thereby improving mechanical power. As a result, improved mechanical power translates into higher hydraulic power, leading to substantially improved water flows. Simulation studies have shown that the proposed approach effectively increases water flow. Specifically, the first case showed a gain of 216 l/h, the second a gain of 432 l/h, and the third a gain of 288 l/h. This improvement holds great promise for promoting sustainable agricultural practices, particularly in regions where access to conventional energy sources is limited. By addressing the challenges posed by PSCs and improving the performance of the SPVWPS, this research may contribute to the advancement of renewable energy technologies in agricultural applications, ultimately helping to achieve the goal of food security and environmental sustainability. In terms of practical feasibility, the proposed system is well-aligned with contemporary hardware capabilities. The required irradiance sensors, one per PV module, are commercially available and cost-effective. The reconfigurable switch matrix—necessary for implementing dynamic topologies—can be realized using microcontroller-controlled relays or MOSFETs, without excessive hardware

complexity. Moreover, the BWO algorithm and KF-based MPPT operate efficiently enough to be executed on embedded systems such as FPGAs or DSPs in real time. This ensures the viability of real-time control and makes the implementation of the proposed technique both practical and scalable for deployment in rural, off-grid settings.

REFERENCES

[1] Chaurey, A., Sadaphal, P.M., Tyaqi, D. (1993). Experiences with SPV water pumping systems for rural applications in India. Renewable Energy, 3(8): 961-964. https://doi.org/10.1016/0960-1481(93)90058-O

[2] Mahmoud, M. (1990). Experience results and techno-economic feasibility of using photovoltaic generators instead of diesel motors for water pumping from rural desert wells in Jordan. IEE Proceedings C (Generation, Transmission and Distribution), 137(6): 391-394. https://doi.org/10.1049/ip-c.1990.0053

[3] Chandel, S.S., Naik, M.N., Chandel, R. (2015). Review of solar photovoltaic water pumping system technology for irrigation and community drinking water supplies. Renewable and Sustainable Energy Reviews, 49: 1084-1099. https://doi.org/10.1016/j.rser.2015.04.083

[4] Patel, H., Agarwal, V. (2008). MATLAB-based modeling to study the effects of partial shading on PV array characteristics. IEEE Transactions on Energy Conversion, 23(1): 302-310. https://doi.org/10.1109/TEC.2007.914308

[5] Loukriz, A., Saigaa, D., Drif, M., Hadjab, M., Houari, A., Messalti, S., Saeed, M.A. (2021). A new simplified algorithm for real-time power optimization of TCT interconnected PV array under any mismatch conditions.

Journal Européen des Systèmes Automatisés, 54(6): 805-817. https://doi.org/10.18280/jesa.540602

[6] Loukriz, A., Drif, M., Bouchelaghem, A., Saigaa, D., Bendib, A., Moadh, K. (2022). Current balancing and PSO methods-based PV array output power optimization: A comparative study. In 2022 International Conference of Advanced Technology in Electronic and Electrical Engineering (ICATEEE), M'sila, Algeria, pp. 1-6. https://doi.org/10.1109/ICATEEE57445.2022.10093690

[7] Kaushika, N.D., Gautam, N.K. (2003). Energy yield simulations of interconnected solar PV arrays. In 2003 IEEE Power Engineering Society General Meeting (IEEE Cat. No.03CH37491), Toronto, ON, Canada, pp. 2618-2618. https://doi.org/10.1109/PES.2003.1271059

[8] Loukriz, A., Kichene, M., Bendib, A., Drif, M., Saigaa, D., Ahmed, H. (2024). Improved dynamic reconfiguration strategy for power maximization of TCT interconnected PV arrays under partial shading conditions. Preprint (Version 1) Research Square. https://doi.org/10.21203/rs.3.rs-3960928/v1

[9] La Manna, D., Vigni, V.L., Sanseverino, E.R., Di Dio, V., Romano, P. (2014). Reconfigurable electrical interconnection strategies for photovoltaic arrays: A review. Renewable and Sustainable Energy Reviews, 33: 412-426. https://doi.org/10.1016/j.rser.2014.01.070

[10] Sahu, H.S., Nayak, S.K., Mishra, S. (2015). Maximizing the power generation of a partially shaded PV array. IEEE Journal of Emerging and Selected Topics in Power Electronics, 4(2): 626-637. https://doi.org/10.1109/JESTPE.2015.2498282

[11] Nguyen, D., Lehman, B. (2008). An adaptive solar photovoltaic array using model-based reconfiguration algorithm. IEEE Transactions on industrial Electronics, 55(7): 2644-2654. https://doi.org/10.1109/TIE.2008.924169

[12] Velasco-Quesada, G., Guinjoan-Gispert, F., Piqué-López, R., Román-Lumbreras, M., Conesa-Roca, A. (2009). Electrical PV array reconfiguration strategy for energy extraction improvement in grid-connected PV systems. IEEE Transactions on Industrial Electronics, 56(11): 4319-4331. https://doi.org/10.1109/TIE.2009.2024664

[13] Matam, M., Barry, V.R., Govind, A.R. (2018). Optimized reconfigurable PV array based photovoltaic water-pumping system. Solar Energy, 170: 1063-1073. https://doi.org/10.1016/j.solener.2018.05.046

[14] Storey, J.P., Wilson, P.R., Bagnall, D. (2012). Improved optimization strategy for irradiance equalization in dynamic photovoltaic arrays. IEEE Transactions on Power Electronics, 28(6): 2946-2956. https://doi.org/10.1109/TPEL.2012.2221481

[15] Manjunath, M., Venugopal Reddy, B., Lehman, B. (2019). Performance improvement of dynamic PV array under partial shade conditions using M2 algorithm. IET Renewable Power Generation, 13(8): 1239-1249. https://doi.org/10.1049/iet-rpg.2018.5675

[16] Esram, T., Chapman, P.L. (2007). Comparison of photovoltaic array maximum power point tracking techniques. IEEE Transactions on Energy Conversion, 22(2): 439-449. https://doi.org/10.1109/TEC.2006.874230

[17] Motahhir, S., Aoune, A., El Ghzizal, A., Sebti, S., Derouich, A. (2017). Comparison between Kalman filter and incremental conductance algorithm for optimizing photovoltaic energy. Renewables: Wind, Water, and Solar, 4(1): 8. https://doi.org/10.1186/s40807-017-0046-8

[18] Baramadeh, M.Y., Abouelela, M.A.A., Alghuwainem, S.M. (2021). Maximum power point tracker controller using fuzzy logic control with battery load for photovoltaics systems. Smart Grid and Renewable Energy, 12(10): 163-181. https://doi.org/10.4236/sgre.2021.1210010

[19] Messalti, S. (2015). A new neural networks MPPT controller for PV systems. In IREC2015 The Sixth International Renewable Energy Congress, Sousse, Tunisia, IEEE, pp. 1-6. https://doi.org/10.1109/IREC.2015.7110907

[20] Abdullah, M.A., Al-Hadhrami, T., Tan, C.W., Yatim, A.H. (2018). Towards green energy for smart cities: Particle swarm optimization based MPPT approach. IEEE Access, 6: 58427-58438. https://doi.org/10.1109/ACCESS.2018.2874525

[21] Mohammad, L., Prasetyono, E., Murdianto, F.D. (2019). Performance evaluation of ACO-MPPT and constant voltage method for street lighting charging system. In 2019 International Seminar on Application for Technology of Information and Communication (iSemantic), Semarang, Indonesia, IEEE, pp. 411-416. https://doi.org/10.1109/ISEMANTIC.2019.8884303

[22] González-Castaño, C., Restrepo, C., Kouro, S., Rodriguez, J. (2021). MPPT algorithm based on artificial bee colony for PV system. IEEE Access, 9: 43121-43133. https://doi.org/10.1109/ACCESS.2021.3066281

[23] Hayyolalam, V., Kazem, A.A.P. (2020). Black widow optimization algorithm: A novel meta-heuristic approach for solving engineering optimization problems. Engineering Applications of Artificial Intelligence, 87: 103249. https://doi.org/10.1016/j.engappai.2019.103249

[24] Houssein, E.H., Helmy, B.E.D., Oliva, D., Elngar, A.A., Shaban, H. (2021). A novel black widow optimization algorithm for multilevel thresholding image segmentation. Expert Systems with Applications, 167: 114159. https://doi.org/10.1016/j.eswa.2020.114159

[25] Baby, T.C., Sabah, V.S., Lall, K.P., Chitra, A. (2015). Multilevel inverter fed induction motor drive for pumping application. In 2015 International Conference on Technological Advancements in Power and Energy (TAP Energy), Kollam, India, pp. 85-92. https://doi.org/10.1109/TAPENERGY.2015.7229597

[26] Lufei, X., Guangqun, N. (2012). Research on direct torque control of induction motor based on TMS320LF2407A. Physics Procedia, 25: 513-519. https://doi.org/10.1016/j.phpro.2012.03.119

[27] Shepovalova, O.V., Belenov, A.T., Chirkov, S.V. (2020). Review of photovoltaic water pumping system research. Energy Reports, 6: 306-324. https://doi.org/10.1016/j.egyr.2020.08.053

[28] Errouha, M., Derouich, A., Nahid-Mobarakeh, B., Motahhir, S., El Ghzizal, A. (2019). Improvement control of photovoltaic based water pumping system without energy storage. Solar Energy, 190: 319-328. https://doi.org/10.1016/j.solener.2019.08.024

[29] Chikh, K., Khafallah, M., Saâd, A. (2012). Improved DTC algorithms for reducing torque and flux ripples of PMSM based on fuzzy logic and PWM techniques. In MATLAB-A Fundamental Tool for Scientific

Computing and Engineering Applications-Volume 1. IntechOpen. https://doi.org/10.5772/48503.

[30] Aissa, O., Moulahoum, S., Kabache, N., Houassine, H. (2014). DTC of induction motor drive fed by NPC three level inverter based on fuzzy logic. In 2014 16th International Conference on Harmonics and Quality of Power (ICHQP), Bucharest, Romania, pp. 214-218. https://doi.org/10.1109/ICHQP.2014.6842911

[31] Periasamy, P., Jain, N.K., Singh, I.P. (2015). A review on development of photovoltaic water pumping system. Renewable and Sustainable Energy Reviews, 43: 918-925. https://doi.org/10.1016/j.rser.2014.11.019

[32] Singla, C., Pahwa, V., Kumar, D. (2016). Optimum MPPT technique for the PV based field oriented control of induction motor feeding centrifugal pump. Indian Journal of Science and Technology, 9: 1-8. https://doi.org/10.17485/ijst/2016/v9i44/101067

[33] Errouha, M., Derouich, A., Motahhir, S., Zamzoum, O., El Ouanjli, N., El Ghzizal, A. (2019). Optimization and control of water pumping PV systems using fuzzy logic controller. Energy Reports, 5: 853-865. https://doi.org/10.1016/j.egyr.2019.07.001

[34] Loukriz, A. (2022). Contribution au développement de techniques de recherche de la topologie optimale d'un générateur photovoltaïque. (Doctoral Dissertation, Faculté des Sciences et de la Technologie). Biskra University. http://thesis.univ-biskra.dz/id/eprint/5806, accessed on Aug. 14, 2023.

[35] Shebani, M.M., Iqbal, T. (2017). Dynamic modeling, control, and analysis of a solar water pumping system for Libya. Journal of Renewable Energy, 2017(1): 8504283. https://doi.org/10.1155/2017/8504283

[36] Saoudi, A., Krim, S., Mimouni, M.F. (2021). Enhanced intelligent closed loop direct torque and flux control of induction motor for standalone photovoltaic water pumping system. Energies, 14(24): 8245. https://doi.org/10.3390/en14248245

[37] Ajmal, A.M., Babu, T.S., Ramachandaramurthy, V.K., Yousri, D., Ekanayake, J.B. (2020). Static and dynamic reconfiguration approaches for mitigation of partial shading influence in photovoltaic arrays. Sustainable Energy Technologies and Assessments, 40: 100738. https://doi.org/10.1016/j.seta.2020.100738

[38] Becerra-Nuñez, G., Castillo-Atoche, A., Vazquez-Castillo, J., Datta, A., Quijano-Cetina, R.G., Peña-Alzola, R., Carrasco-Alvarez, R., Osorio-De-La-Rosa, E. (2020). An FPGA Kalman-MPPT implementation adapted in SST-based dual active bridge converters for DC microgrids systems. IEEE Access, 8: 202946-202957. https://doi.org/10.1109/ACCESS.2020.3033718

[39] Tang, Q., Ge, X., Liu, Y.C., Hou, M. (2018). Improved switching-table-based DTC strategy for the post-fault three-level NPC inverter-fed induction motor drives. IET Electric Power Applications, 12(1): 71-80. https://doi.org/10.1049/iet-epa.2017.0354

NOMENCLATURE

Abbreviation	Definition
PV	Photovoltaic
BWO	Black Widow Optimization
IC	Incremental Conductance
IMs	Induction Motors
GMPP	Global MPP
PSO	Particle Swarm Optimization
PSCs	Partial Shading Conditions
LMPPs	Local MPPs
KF	Kalman Filter
Q	Water Discharge
MPPT	Maximum power point tracking
P&O	Perturb and Observe (P&O)
PS	Partial shading
PV	Photovoltaic
SPVWPS	Solar Photovoltaic Water Pumping System
PS	Partial shading
ACO	Ant Colony Optimization
TCT	Total-cross-tied
DTC	Direct Torque Control
Te	Electromagnetic Torque